

## Electronic Supplementary Information (ESI)

### Structural Variations vs Energy Loss in Regioregular Narrow

### Band Gap Polymer Solar Cells

Jianyu Yuan,<sup>a,b</sup> Niva A. Ran,<sup>b</sup> Michael J. Ford,<sup>b</sup> Ming Wang,<sup>\*,b</sup> Mahesh Kumar Ravva,<sup>c</sup> Cheng-Kang Mai,<sup>b</sup> Xiaofeng Liu,<sup>b</sup> Jean-Luc Brédas,<sup>\*,c</sup> Thuc-Quyen Nguyen,<sup>\*,b</sup> Wanli Ma,<sup>\*,a</sup> Guillermo C. Bazan<sup>\*,b</sup>

<sup>a</sup>Jiangsu Key Laboratory for Carbon-Based Functional Materials & Devices, Institute of Functional Nano & Soft Materials (FUNSOM), Soochow University

<sup>b</sup>Center for Polymers and Organic Solids, <sup>§</sup>Department of Chemistry and Biochemistry, <sup>¶</sup>Materials Department, University of California, Santa Barbara

<sup>¶</sup>KAUST Solar Center, Division of Physical Science and Engineering, King Abdullah University of Science and Technology, Thuwal 23955-6900, Saudi Arabia

Email: [mwang@chem.ucsb.edu](mailto:mwang@chem.ucsb.edu) (M. Wang), [jean-luc.bredas@kaust.edu.sa](mailto:jean-luc.bredas@kaust.edu.sa) (J.-L. Brédas), [quyen@chem.ucsb.edu](mailto:quyen@chem.ucsb.edu) (T.-Q. Nguyen), [wlma@suda.edu.cn](mailto:wлма@suda.edu.cn) (W. Ma), [bazan@chem.ucsb.edu](mailto:bazan@chem.ucsb.edu) (G.C. Bazan)

#### Content

1. General methods
2. Synthesis and characterizations
3. Thermogravimetric analysis and differential scanning calorimetry
4. UV-vis absorption
5. Cyclic voltammetry
6. Mobility measurements by space charge limited current method
7. Grazing incidence wide angle X-ray scattering
8. Solar cell performance
9. TD-DFT calculation

## 1. General methods

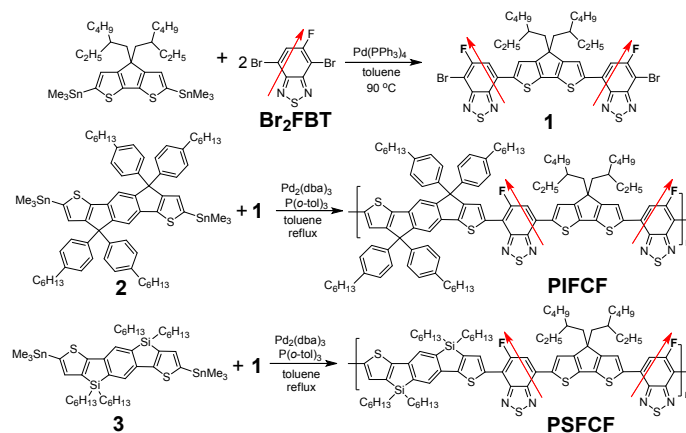
Ultraviolet-Visible (UV-Vis) absorption spectra were recorded on a DU-800 spectrometer. Nuclear magnetic resonance (NMR) spectra were obtained on Varian 500 MHz spectrometer. Gel permeation chromatography (GPC) was performed in chloroform ( $\text{CHCl}_3$ ) on a Waters 2690 Separation Module equipped with a Waters 2414 Refractive Index Detector and a Waters 2996 Photodiode Array Detector. Molecular weights were calculated relative to linear PS standards. Thermogravimetric analysis (TGA) was carried out using a Perkin Elmer TGA4000 instrument with about 3-5 mg polymer samples at a rate of 10 °C / min in the temperature range of 25 to 700 °C. Differential scanning calorimetry (DSC) was determined by a TA Instruments DSC (Model Q-20) with about 3-5 mg polymer samples at a rate of 10 °C / min in the temperature range of 30 to 300 °C. Cyclic voltammetry (CV) measurements were conducted using a standard three-electrode configuration under an argon atmosphere. A three-electrode cell was equipped with a glassy carbon working electrode, an Ag wire reference electrode and a Pt wire counter-electrode. The measurements were performed in absolute acetonitrile with tetrabutylammoniumhexafluorophosphate (0.1 M) as the supporting electrolyte at a scan rate of 100 mV/s. Polymer films for CV test were drop-casted onto the glassy carbon working electrode from a 5 mg/mL chloroform solution. The absolute energy level of ferrocene/ferrocenium ( $\text{Fc}/\text{Fc}^+$ ) to be 4.8 eV below vacuum. Atomic force microscopy (AFM) was conducted on an Asylum Research MFP 3D AFM, transmission electron microscopy (TEM) images were obtained using a Veeco Multimode V instrument and Tecnai T2 transmission electron microscope. 2D grazing-incidence wide-angle X-ray scattering (GIWAXS) measurements were performed at the Stanford Synchrotron Radiation Lightsource (SSRL) on Beamline 11-3, with a MAR345 image plate area detector, at 12.7 keV incident photon energy, and at incident angles of 0.12°. Thin film illumination occurred in a helium atmosphere to minimize X-ray beam damage.

Experimental section for EQE/EL: EQE characteristics were measured in a nitrogen-filled glovebox using a setup consisting of a 75 W Xe light source, monochromator,

optical chopper, lock-in amplifier, and a National Institute of Standards and Technology calibrated silicon photodiode for power-density calibration. To obtain sub-bandgap EQE, higher sensitivity settings were used with a longer time delay between measurement points. Electroluminescence spectra for the bilayers were collected directly from the solar cell devices, by applying a bias that is close to the turn-on voltage of the devices. The resulting emission was collected with a Si CCD camera cooled to  $-70^{\circ}\text{C}$ . The spectra were corrected for detector response using a blackbody spectrum.

All DFT calculations were carried out using the long-range corrected  $\omega\text{B97X-D}$  functional with the 6-31G(d,p) basis set. The randomly generated donor:acceptor complexes were optimized in the gas phase at the  $\omega\text{B97X-D}/6\text{-}31\text{G(d,p)}$  level of theory. Excited-state energies were calculated at the TD-DFT level using the Tamm-Dancoff approximation and considering the ground-state geometries. The impact of the surrounding dielectric medium (electron polarization effects) on  $E_{\text{CT}}$  was taken into account by combining the DFT calculations with the polarizable continuum model (PCM). Furthermore, the range separation parameter  $\omega$  of the  $\omega\text{B97XD}$  functional is optimally tuned in the presence of the dielectric medium; all excited-state calculations were carried out with the PCM-tuned  $\omega$  value. All DFT calculations reported here were performed with the Gaussian 09 package.<sup>4</sup>

## 2. Synthesis and characterizations



Scheme S1. Synthesis of PIFCF and PSFCF.

4,7-Dibromo-5-fluorobenzo[*c*][1,2,5]thiadiazole and benzo[1,2-*b*:4,5-*b'*]bis-2-bromo-4,4'-dihexyl-4*H*-silolo[3,2-*b*]thiophene) were purchased from 1-Materials Co. Tris(dibenzylideneacetone)dipalladium (0) [Pd<sub>2</sub>(dba)<sub>3</sub>] and tri-*o*-tolylphopine [P(*o*-tol)<sub>3</sub>] and tetrakis(triphenylphosphine)palladium(0) [Pd(PPh<sub>3</sub>)<sub>4</sub>] were purchased from Strem Chemicals Inc. Compound 5,5'-bis(trimethylstannyl)-4,4-bis(2-ethylhexyl)cyclopenta-[2,1-*b*: 3,4-*b'*]-dithiophene (bis-CPDT-tin)<sup>1</sup>, {4,4,9,9-Tetrakis(4-hexylphenyl)-4,9-dihydro-*s*-indaceno[1,2-*b*:5,6-*b'*]dithiophene-2,7-diyl}bis(trimethylstannane) (**2**)<sup>2</sup> benzo[1,2-*b*:4,5-*b'*]bis(2-trimethylstannyl-4,4'-dihexyl-4*H*-silolo[3,2-*b*]thiophene) (**3**)<sup>3</sup> were prepared by methods similar to those reported in the literature. All the solvents were distilled before used.

5,5'-bis{(4-(6-fluoro-7-bromo-[1,2,5]thiadiazolobenzene))-{4,4-bis(2-ethylhexyl)cyclopenta-[2,1-*b*: 3,4-*b'*]-dithiophene} (**1**): A 20 mL reaction vial was charged with bis-CPDT-tin (500 mg, 0.687 mmol, 1.0 eq), 4,7-Dibromo-5-fluorobenzo[*c*][1,2,5]thiadiazole (535 mg, 1.717 mmol, 2.5 eq), Pd(PPh<sub>3</sub>)<sub>4</sub> (80 mg, 0.069 mmol, 0.10 eq), and dry toluene (15 mL) inside a dry nitrogen box. The reaction vial was then sealed using a Teflon<sup>®</sup> cap and moved out of the dry box. The reaction mixture was stirred at 90 °C in a conventional oil bath for 72 h. The resulting mixture was first passed through a short silica gel column by using chloroform as

eluent. After the chloroform solution was concentrated to dryness, a second purification step via column chromatography (10~30% DCM in hexane gradient) was needed to give analytically pure **1** (356 mg, 60%) as a dark powder.  $^1\text{H}$  NMR ( $\text{CDCl}_3$ , 500 MHz,  $\delta$ ) 8.15 (s, 2H), 7.72 (d, 2H), 2.13-2.04 (m, 4H), 1.08-0.80 (m, 18H), 0.68-0.65 (m, 12H).  $^{13}\text{C}$  NMR ( $\text{CDCl}_3$ , 500 MHz,  $\delta$ ): 161.9, 159.9, 159.8, 154.4, 154.3, 148.2, 140.1, 138.5, 128.2, 128.1, 124.3, 114.7, 114.4, 95.5, 95.3, 54.5, 43.2, 35.4, 34.3, 28.6, 27.5, 22.8, 14.0, 10.7.

**PIFCF**: **1** (86.5 mg, 0.1 mmol), **2** (123.3 mg, 0.1 mmol), tri(*o*-tolyl)phosphine (8 mg, 0.032 mmol), and  $\text{Pd}_2(\text{dba})_3$  (4 mg, 0.004 mmol) were dissolved in 5/0.5 mL dry toluene/DMF under argon. After stirred at 110 °C for 1 h, the mixture become very sticky and hardly to be stirred, after kept at 110 °C for 24 h, the mixture was cooled to room temperatures and precipitated in methanol (70 mL). The precipitate was filtered and washed with methanol (12 h) and hexane (12 h) successively in a soxhlet apparatus to remove oligomers and catalyst residue. Finally, the polymer was extracted with chloroform (24 h). The chloroform fraction was concentrated and precipitated in methanol. The polymer was precipitated and collected via filter paper, dried over in the vacuum line to give 150 mg dark solid, yield 89%.  $^1\text{H}$  NMR ( $\text{CDCl}_3$ , 500 MHz,  $\delta$ ) 8.25 (m, 2H), 8.10 (m, 2H), 7.72 (m, 4H), 7.58 (m, 2H), 7.28 (m, 8H) 7.11 (m, 8H), 2.58 (m, 6H) 2.04 (br, 2H), 1.55-0.65 (br, 76H);  $M_n = 17,000$  g/mol,  $M_w = 28,600$  g/mol,  $PDI = 1.7$ .

**PSFCF**: **1** (86.5 mg, 0.1 mmol), **3** (96.1 mg, 0.1 mmol),  $\text{Pd}(\text{PPh}_3)_4$  (5.8 mg, 0.005 mmol), xylene (2 mL) were added to a 2-5 mL microwave tube in the nitrogen atmosphere glovebox. The tube was and subjected to the following reaction conditions in the microwave reactor: 80 °C for 2 min, 130 °C for 2 min, 160 °C for 2 min, 185 °C for 2 min and 200 °C for 40 min. The reaction was allowed to cool to room temperature, the polymer was precipitated in methanol. The precipitates were collected by a cellulose extraction thimble and extracted with methanol, hexane, dichloromethane and chloroform respectively via a Soxhlet extractor. The chloroform solution was concentrated under vacuum. Then concentrated polymer solution was dropwise to the methanol under the stirring. The polymer was precipitated and collected via

filter paper, dried over in the vacuum line to give 100 mg dark solid, yield 72 %.  $^1\text{H}$  NMR ( $\text{CDCl}_3$ , 500 MHz,  $\delta$ ) 8.34 (br, 2H), 8.14 (br, 2H), 7.76 (br, 4H) 1.49-0.80 (br, 62H), 0.69 (m, 24H);  $M_n = 36,000$  g/mol,  $M_w = 57,600$  g/mol,  $PDI = 1.6$ .

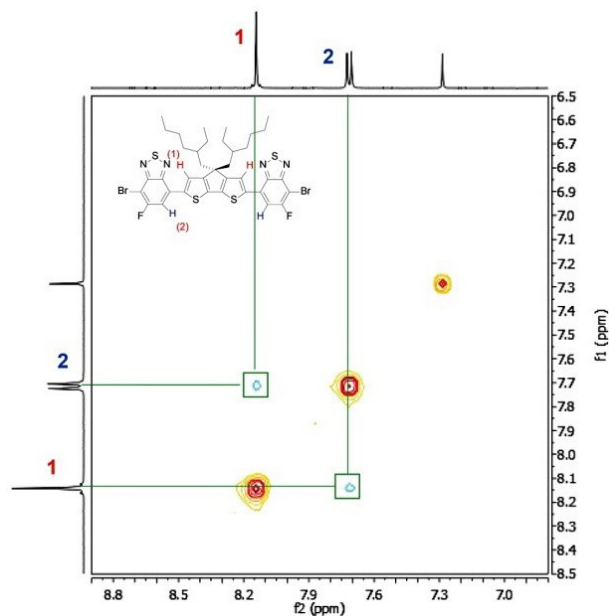


Figure S1. Aromatic region (8.9 ~ 6.8 ppm) of 2D  $^1\text{H}$ - $^1\text{H}$  NOESY NMR spectrum of 1 and 2 in  $\text{CDCl}_3$  at room temperature with a concentration of ca.35 mg/mL. Crosspeaks(blue)indicates the spatial interaction between H1and H2, due to fast rotation of the C-C single bond between two aromatic units.

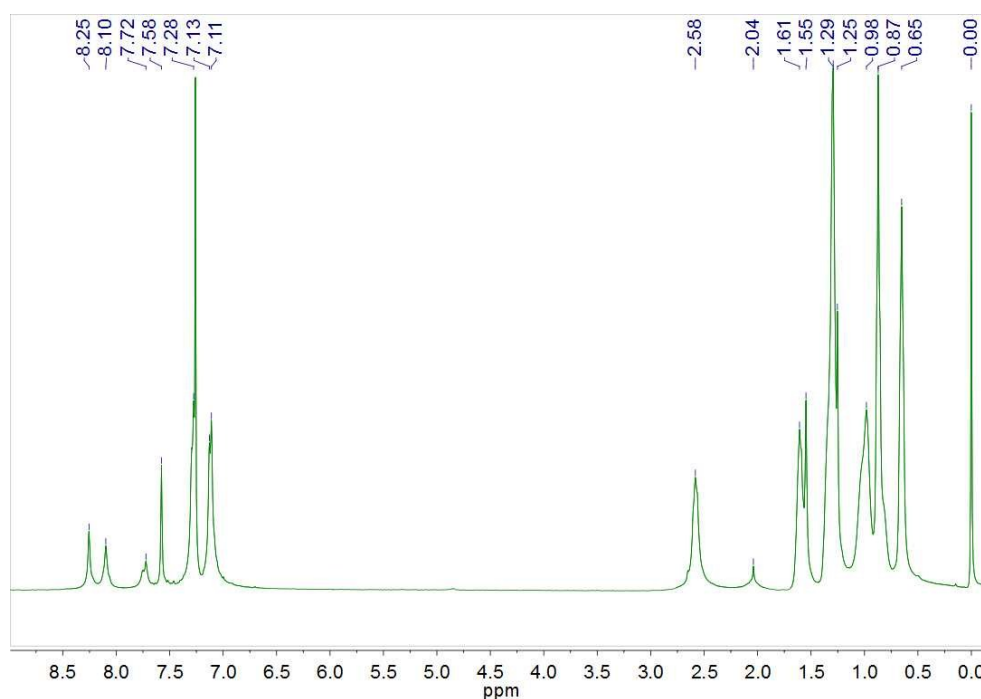


Figure S2.  $^1\text{H}$  NMR spectrum of PIFCF in  $\text{CDCl}_3$

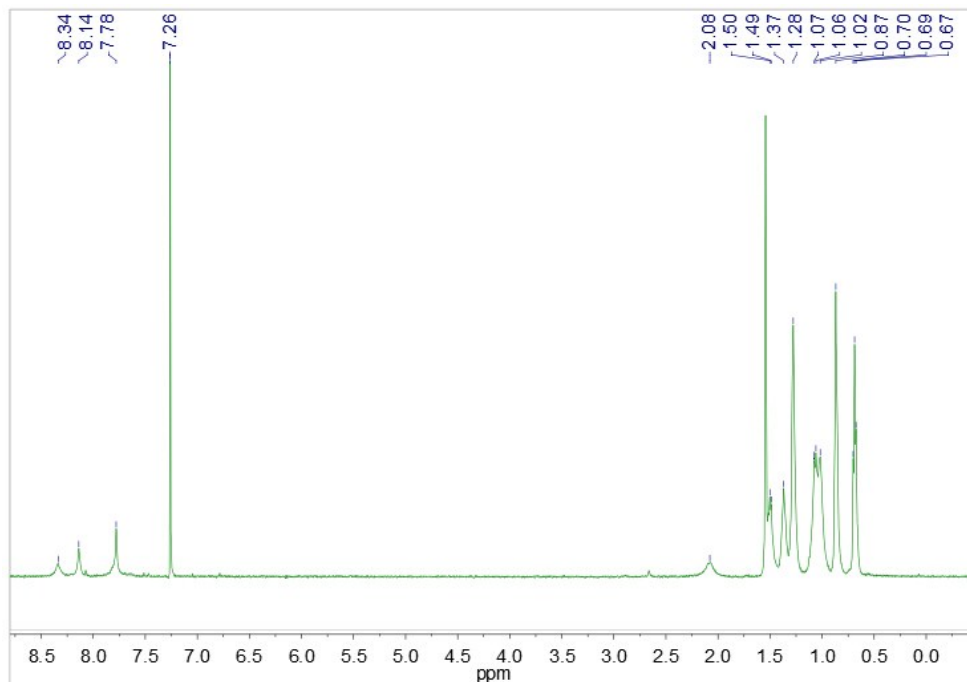


Figure S3.  $^1\text{H}$  NMR spectrum of PSFCF in  $\text{CDCl}_3$

### 3. Thermogravimetric analysis and Differential scanning calorimetry

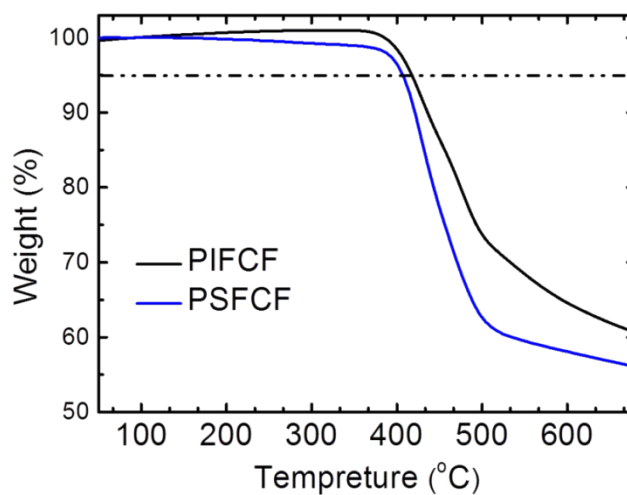


Figure S4. Thermogravimetric analysis with a heating rate of  $10\text{ }^\circ\text{C}/\text{min}$  under an inert atmosphere ( $\text{N}_2$ ), the dash line indicates 95% decomposition.

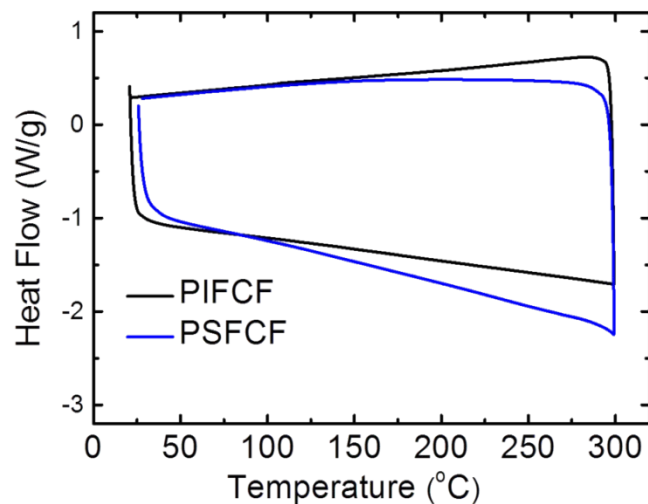


Figure S5. Differential scanning calorimetry curves with a heating rate of 10 °C/min under an inert atmosphere (Ar).

#### 4. UV-vis absorption

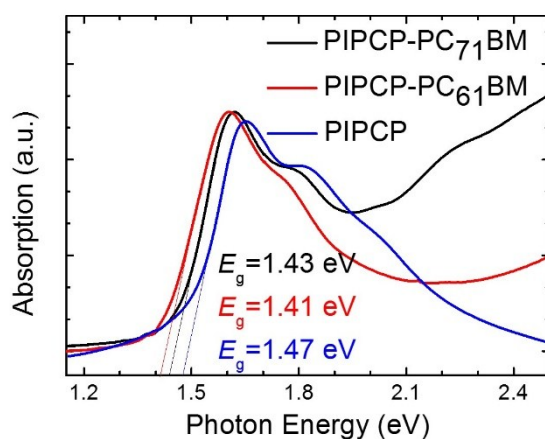


Figure S6. Film absorption of PIPCP and with fullerene blend films.

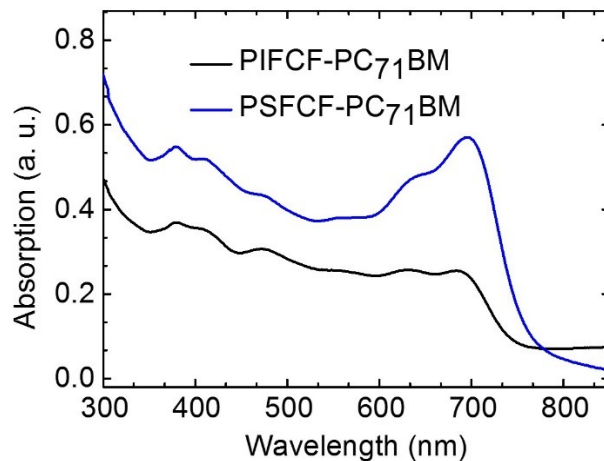




Figure S7. FBT analogues with PC<sub>71</sub>BM blend films on quartz substrates (Both blend films were prepared according to the optimal device condition: polymer:PC<sub>71</sub>BM=2:1, chloroform with optimal DIO, the thickness is around 100 nm).

## 5. Cyclic voltammetry

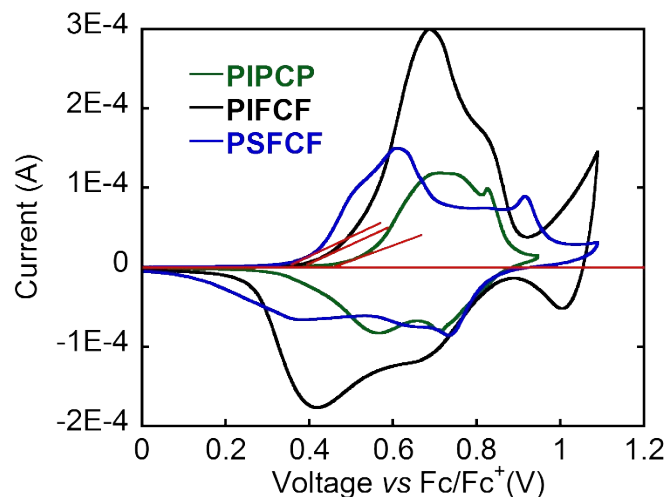


Figure S8. Oxidation onsets of polymers PIPCP, PIFCF and PSFCF.

## 6. Mobility measurements by space charge limited current method

Hole-only and electron-only devices were fabricated to measure the hole and electron mobilities using the space charge limited current (SCLC) method. The hole-only device structure is ITO/PEDOT:PSS/polymer/Au (50 nm) and the electron-only device structure is ITO/ZnO/Polymer:PC<sub>71</sub>BM /LiF (0.6 nm)/Al. The thickness was measured by Profilometer. The mobility was determined by fitting the dark current to the model of a single carrier SCLC, which is described by the equation:

$$J = \frac{9}{8} \varepsilon_0 \varepsilon_r \mu \frac{V^2}{d^3},$$

where  $J$  is the current,  $\varepsilon_0$  is the permittivity of free space,  $\varepsilon_r$  is the relative permittivity of the material,  $\mu$  is the zero-field mobility,  $d$  is the thickness of the polymer layer,  $V$  is the applied voltage. Then mobilities were calculated from the fitting slope of the  $J^{1/2}$ - $V$  curves below:

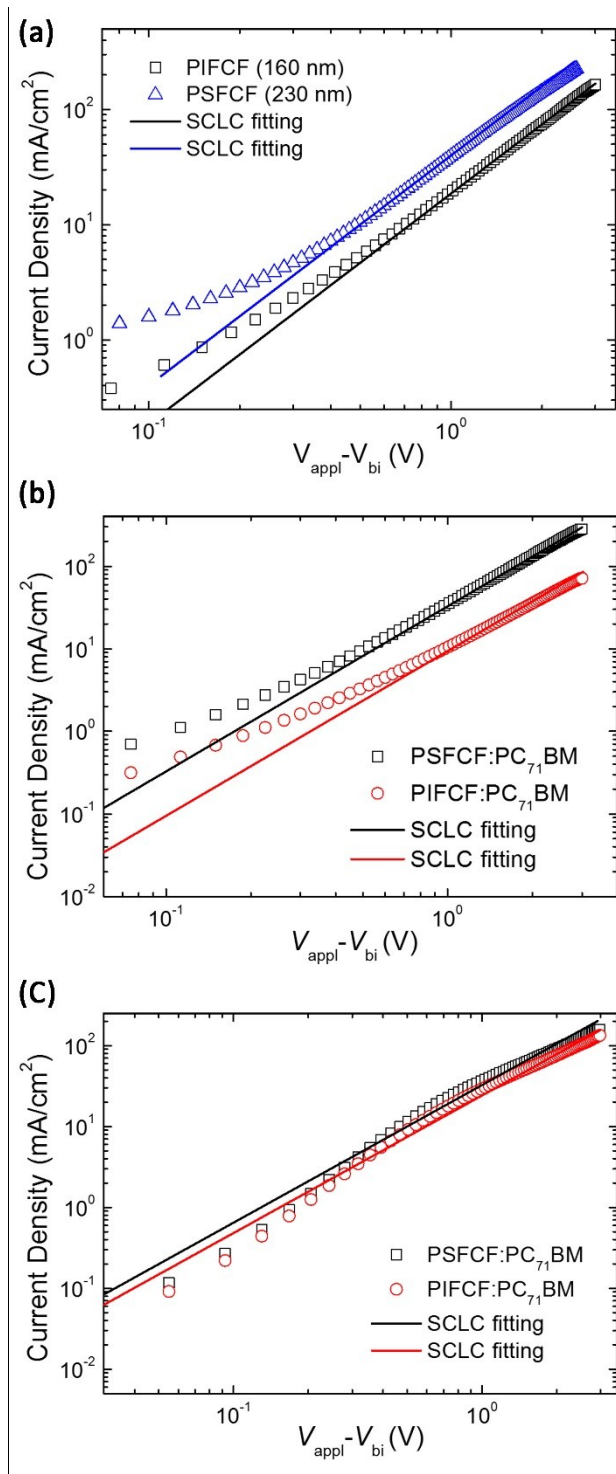


Figure S9.  $J$ - $V$  curves of: (a) neat polymer films hole-only diodes devices; (b) blend films hole-only diodes devices; (c) blend films electron-only diodes devices. (The solid SCLC fitting lines' slopes are 2).

## 7. Grazing incidence wide angle X-ray scattering

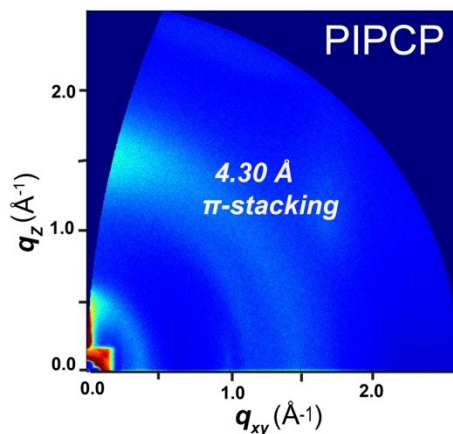


Figure S10. Neat PIPCP film cast from chloroform.

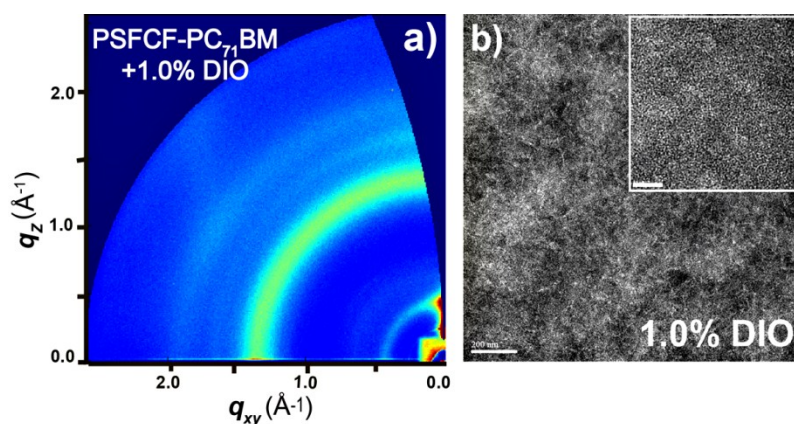


Figure S11. 2D-GIWAXS pattern(a) and TEM image (b) of optimal PSFCF:PC<sub>71</sub>BM blend film.

*Crystal correlation length estimates (Scherrer analysis):*

The crystal correlation lengths (CCL) were estimated by the following equation:

$$CCL = \frac{2\pi}{FWHM}$$

Where FWHM is the full-width-at-half-maximum of the fitted Gaussian

Table S1. Summary of polymer CCL values

	Processing Solvent	(100) ( $Q_z$ )	(010) ( $Q_z$ )	(100) ( $Q_{xy}$ )
PIFCF	CF	1.7 nm	1.5 nm	5.2 nm
PSFCF	CF	2.6 nm	2.6 nm	4.0 nm
PIPCP	CF	2.7 nm	1.2 nm	3.8 nm

## 8. Solar Cells Performance

*Device Fabrication:* Solution-processed solar cells devices were fabricated with a conventional architecture of ITO/PEDOT:PSS/active layer/Ca/Al, an inverted structure of ITO/ZnO/active layer/MoO<sub>x</sub>/Ag, respectively. The ITO-coated glass substrates were firstly cleaned by ultrasonic treatment in detergent, deionized water, acetone and isopropyl alcohol for 30 minutes each, and subsequently dried in an oven overnight. After treated with UV/ozone for 30 min, PEDOT:PSS (Al 4083) layer was deposited and dried at 150 °C in ambient atmosphere for 10 mins, ZnO (so-gel method)<sup>4</sup> layer was deposited and dried at 200 °C in ambient atmosphere for 10 mins. Active layers were spun at varying spin rate from Polymer:PC<sub>71</sub>BM solutions at different weight ratio, cathodes were deposited by sequential thermal evaporation of 10 nm of calcium followed by 80 nm of aluminum, for the inverted devices, cathodes were deposited by sequential thermal evaporation of 5 nm of MoO<sub>x</sub> followed by 80 nm of silver. The device area was 4.5 mm<sup>2</sup>.

*Device Characterization :* Photovoltaic characterization was performed on a Keithley 2602 source measure unit with a 300 W Xe arc lamp and an AM 1.5 global filter. The solar simulator illumination intensity was measured using a KG1 filter from the National Renewable Energy Laboratory (NREL) with a silicon photovoltaic. EQE spectra were measured using a 75 W Xe lamp, Newport monochrometer, Newport optical chopper, and a Stanford Research Systems lock-in amplifier. Power-density calibration was done by National Institute of Standards and Technology traceable silicon photodiode.

Table S2. Performance of PIFCF under the conventional structure using different solvents. (ITO/PEDOT:PSS/ PIFCF:PC<sub>71</sub>BM /Ca/Al, each condition average result is based on five devices. CF: chloroform (16 mg/mL); TA: thermal annealing at 120 °C for 10 min)

Blend Ratio	V <sub>oc</sub> (V)	J <sub>sc</sub> (mA/cm <sup>2</sup> )	FF	PCE (%) Average	PCE (%) Best
1:1	0.86	3.63	0.38	1.15	1.19
1:1 + 1.0% DIO	0.79	2.20	0.36	0.60	0.63

1:2	0.83	7.46	0.45	2.68	2.79
1:2 + TA	0.83	7.38	0.44	2.60	2.70
1:2 +0.5 % DIO	0.83	6.99	0.46	2.57	2.67
1:2 + 1.0 % DIO	0.81	6.66	0.39	2.04	2.10
1:3	0.83	6.11	0.42	2.02	2.13
1:3+1.0 % DIO	0.81	4.99	0.41	1.60	1.65

Table S3. Performance of PSFCF in different D/A ratio.

(ITO/PEDOT:PSS/PSFCF:PC<sub>71</sub>BM (CF solution 16 mg/mL)/Ca/Al, each condition average result is based on five devices.)

D/A ratio	$V_{oc}$ (V)	$J_{sc}$ (mA/cm <sup>2</sup> )	$FF$	$PCE$ (%) Average	$PCE$ (%) Best
1:1+0.5% DIO	0.78	8.87	0.32	2.17	2.21
1:1+1.0% DIO	0.78	15.02	0.57	6.50	6.67
1:1+2.0% DIO	0.78	13.73	0.57	5.76	6.05
1:2+CF	0.82	9.35	0.40	3.00	3.06
1:2+0.5% DIO	0.78	10.86	0.56	4.52	4.73
1:2+1.0% DIO	0.78	15.35	0.60	6.93	7.20

Table S4. Optimized device performance based on PSFCF with different DIO additive content. (ITO/PEDOT:PSS/PSFCF:PC<sub>71</sub>BM/Ca/Al)

DIO (%)	$V_{oc}$ (V)	$J_{sc}$ (mA/cm <sup>2</sup> )	$FF$	$PCE$ (%) Average	$PCE$ (%) Best
PSFCF 0.0	0.82	9.35	0.40	3.00	3.06
PSFCF 0.5	0.78	10.86	0.56	4.52	4.73
PSFCF 1.0	0.78	15.35	0.60	6.93	7.20
PSFCF 2.0	0.78	12.96	0.53	5.17	5.32
PSFCF 3.0	0.78	11.30	0.53	4.56	4.70

Table S5. Device performance based on PSFCF:PC<sub>71</sub>BM blend (w/w, 1/2, chloroform+1.0 % DIO, 16 mg/mL, 1750 rpm) with different molecular weight under the same processing conditions. (ITO/PEDOT:PSS/PSFCF:PC<sub>71</sub>BM/Ca/Al)

$M_n$	$\bar{D}$	$V_{oc}$ (V)	$J_{sc}$ (mA/cm <sup>2</sup> )	$FF$ (%)	$PCE$ (%)
18 k	2.2	0.80	14.81	55.3	<b>6.55</b>
36 k	1.6	0.78	15.02	56.9	<b>6.67</b>

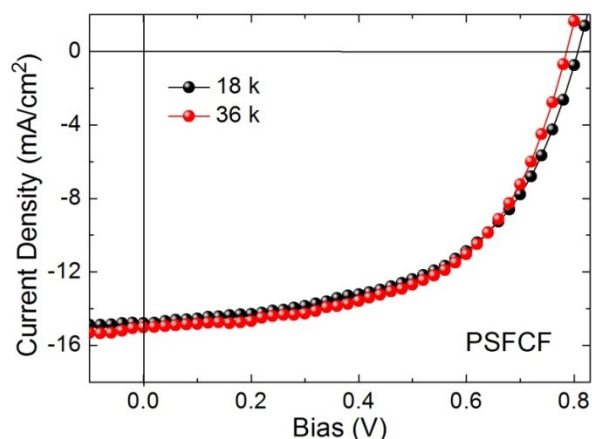


Figure S12. *J-V* curves of PSFCF:PC<sub>71</sub>BM blend with different molecular weight.

Table S6. Device performance based on PIFCF:PC<sub>71</sub>BM (w/w, 1/2, chloroform, 16 mg/mL, 1750 rpm) and PSFCF:PC<sub>71</sub>BM blend (w/w, 1/2, chloroform+1.0 % DIO, 16 mg/mL, 1750 rpm) with different device structure. (Conventional: ITO/PEDOT:PSS/PSFCF:PC<sub>71</sub>BM/Ca/Al; Inverted: ITO/ZnO/active layer/MoO<sub>x</sub>/Ag).

Blend Ratio	Device	$V_{oc}$ (V)	$J_{sc}$ (mA/cm <sup>2</sup> )	FF	PCE (%) Average	PCE (%) Best
PIFCF:PC <sub>71</sub> BM	Conventional	0.83	7.46	0.45	2.68	2.79
PIFCF:PC <sub>71</sub> BM	Inverted	0.83	7.90	0.43	2.70	2.80
PSFCF:PC <sub>71</sub> BM	Conventional	0.78	15.35	0.60	6.93	7.20
PSFCF:PC <sub>71</sub> BM	Inverted	0.79	15.40	0.66	7.80	8.00

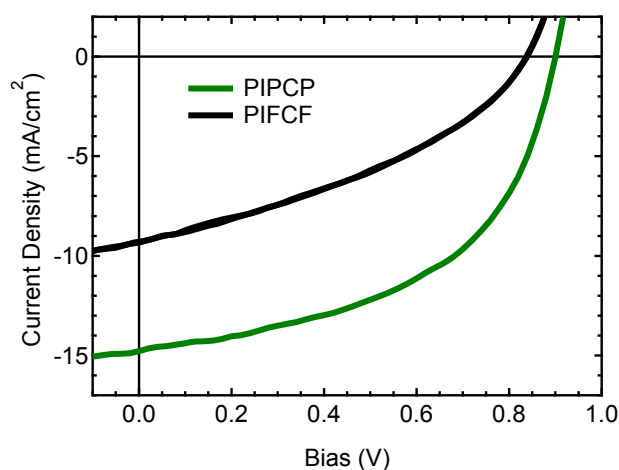


Figure S13. *J-V* curves of PIFCF:PC<sub>61</sub>BM and PIPCP:PC<sub>61</sub>BM inverted devices.

## 9. TD-DFT calculations

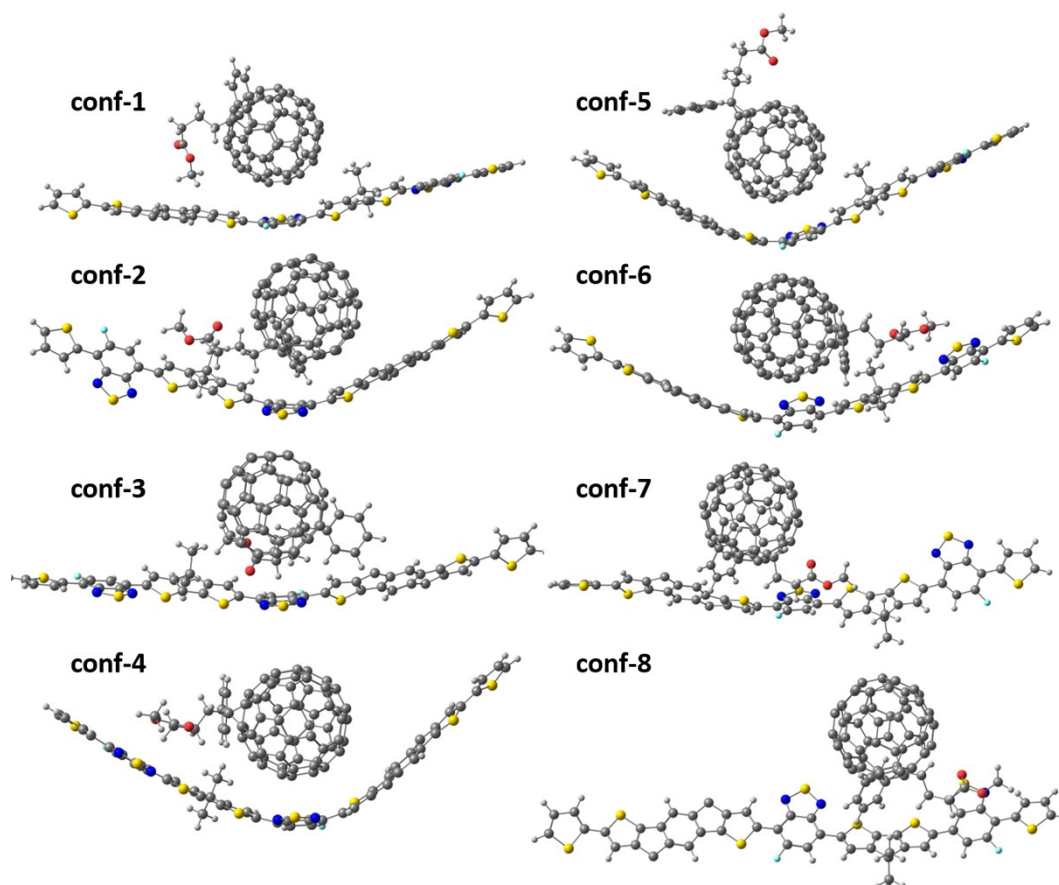


Figure S14. The eight configurations used to calculate the excitation energies of  $S_1$  and  $E_{ct}$  in Figure 7 in the main text. These configurations were randomly generated by placing the fullerene molecule at many different positions around the polymer backbone.

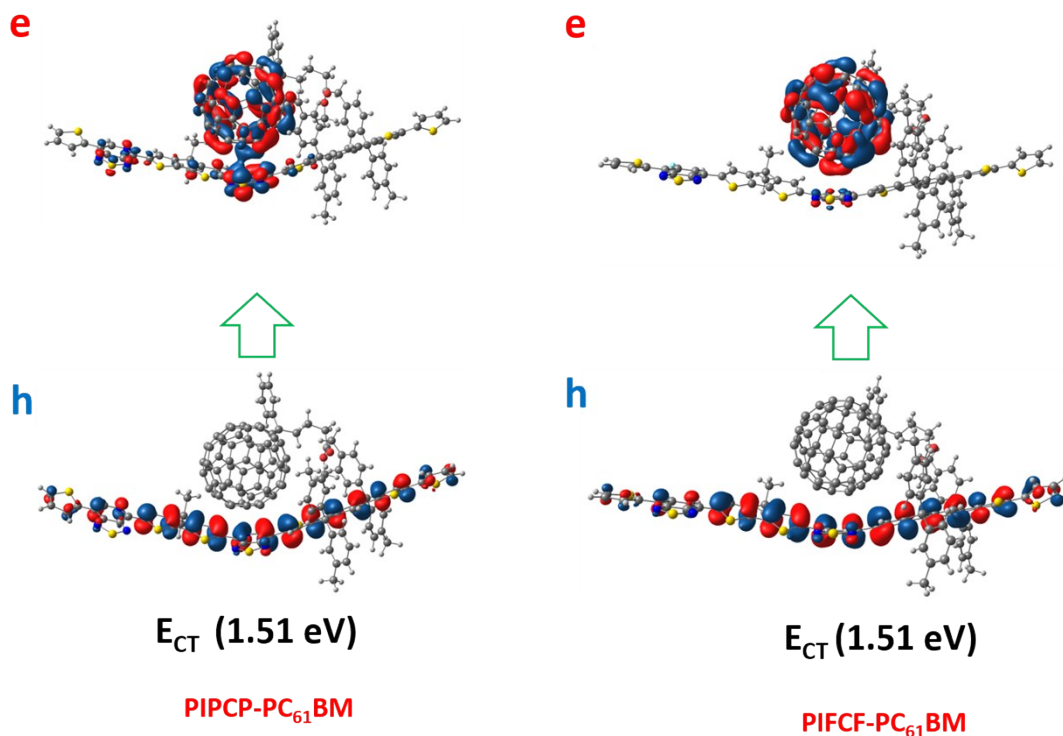


Figure S15. Natural transition orbitals for hole (h) and electron (e) in the lowest CT state for: (left) PIPCP:PC<sub>61</sub>BM and (right) PIFCF:PC<sub>61</sub>BM.

## References

1. J. You, L. Dou, , K. Yoshimura, T. Kato, K. Ohya, T. Moriarty, K. Emery, C.-C. Chen, J. Gao, G. Li, Y. Yang, *Nat. Commun.* 2013, **4**, 1446.
2. Y. C. Chen, C. Y. Yu, Y. L. Fan, L. I. Hung, C. P. Chen, C. Ting, *Chem. Commun.* 2010, **46**, 6503.
3. J. A. Love, I. Nagao, Y. Huang, M. Kuik, V. K. Gupta, C. J. Takacs, J. E. Coughlin, L. Qi, T. S. van der Poll, E. J. Kramer, A. J. Heeger, T.-Q. Nguyen, G. C. Bazan, *J. Am. Chem. Soc.* 2014, **136**, 3597.
4. Y. Sun, J. H. Seo, C. J. Takacs, J. Seiffter, A. J. Heeger, *Adv. Mater.* 2011, **23**, 1679.
5. M. J. Frisch, G. W. Trucks, H. B. Schlegel, G. E. Scuseria, M. A. Robb, J. R. Cheeseman, G. Scalmani, V. Barone, B. Mennucci, G. A. Petersson, H. Nakatsuji, M. Caricato, X. Li, H. P. Hratchian, A. F. Izmaylov, J. Bloino, G. Zheng, J. L. Sonnenberg, M. Hada, M. Ehara, K. Toyota, R. Fukuda, J. Hasegawa, M. Ishida, T. Nakajima, Y. Honda, O. Kitao, H. Nakai, T. Vreven, J. A. Montgomery Jr., J. E. Peralta, F. Ogliaro, M. J. Bearpark, J. Heyd, E. N. Brothers, K. N. Kudin, V. N. Staroverov, R. Kobayashi, J. Normand, K. Raghavachari, A. P. Rendell, J. C. Burant, S. S. Iyengar, J. Tomasi, M. Cossi, N. Rega, N. J. Millam, M. Klene, J. E. Knox, J. B. Cross, V. Bakken, C. Adamo, J. Jaramillo, R. Gomperts, R. E. Stratmann, O. Yazyev, A. J. Austin, R. Cammi, C. Pomelli, J. W. Ochterski, R. L. Martin, K. Morokuma, V. G. Zakrzewski, G. A. Voth, P. Salvador, J. J. Dannenberg, S. Dapprich, A. D. Daniels, Ö. Farkas, J. B. Foresman, J. V. Ortiz, J. Cioslowski, D. J. Fox, *Gaussian 09*; Gaussian, Inc.: Wallingford, CT, USA, 2009.